Stabilizing rôle of a curvature correction to line tension

RICCARDO ROSSO, MARCO VERANI

Stabilizing rôle of a curvature correction to line tension

Riccardo Rosso[a] and Marco Verani[b]

20th December 2007

[a] Dipartimento di Matematica and CNISM, Università di Pavia, Via Ferrata 1, I-27100 Pavia, Italy (`riccardo.rosso@unipv.it`).
[b] MOX - Modelling and Scientific Computing - Dipartimento di Matematica "F. Brioschi", Politecnico di Milano, Milano, Italy (`marco.verani@polimi.it`)

Abstract

We study the effects that a curvature correction to a bare value of the line tension has on the equilibrium and stability of droplets laid upon a rigid substrate. In the simple case of cylindric liquid bridges we prove that even a tiny curvature correction prevents the onset of wildly oscillating perturbations that would make the contact line unstable if a negative line tension were present alone. However, if the curvature correction is not large enough, unstable modes can persist that are not related to the classical Rayleigh instability.

Keywords: line tension, wetting, curvature corrections, shape calculus.
AMS subject classification: 76B45

1   Introduction

Since Gibbs' fundamental paper [1] on the equilibrium of heterogeneous substances, there has been an increasing interest in modelling both the statics and the dynamics of multiphase bodies. In particular, a faithful description of the interface separating two different phases has been sought along different lines originating from either the continuum point of view or the microscopic point of view that relies upon statistical mechanics. In his original approach Gibbs modelled the thin interfacial *three*-dimensional region where the physical properties of two adjoining phases rapidly change as a *two* dimensional surface, called the *dividing* surface, that separates two bulk regions where the phases are *homogeneous*. In general, extensive properties like energy or entropy differ in the real system and in the idealized one. Gibbs ascribed the excess energy or entropy to the dividing surface, adding surface energy and entropy to the bulk terms characterizing the homogeneous phases. The simplest surface energy introduced by Gibbs is proportional to the area of the dividing surface, the constant of proportionality—called the *surface tension*—being positive for stability reasons. Gibbs clearly stated that the surface energy he envisaged was appropriate only for *flat* or weakly curved interfaces, while in the

general case other contributions depending on the interface curvature should enter the energy balance. It was Tolman [2] who first analysed curvature corrections by expanding the surface tension pertaining to a spherical interface of radius R in powers of $1/R$. The length-scale at which this correction is relevant is the *Tolman length* δ_T that has been found to be a molecular length both in numerical simulations [3] of Lennard-Jones fluids and in the analytic treatment of Ref. [4].

A general format to incorporate curvature corrections in the surface energy was sketched by Gibbs himself and later exploited, for instance, in [5] where the following expression for the surface tension

$$\gamma = \gamma_0 + \kappa(c_0 H + \frac{1}{2}H^2) + \hat{\kappa}K \tag{1}$$

was proposed, in which γ_0 is the surface tension for a flat interface, c_0 is the *spontaneous curvature* of the interface, H and K are the *total* and the *Gaussian* curvatures of the interface, while the constitutive parameters κ and $\hat{\kappa}$ are *bending rigidities*. We record here that the Tolman length can be expressed as [5]

$$\delta_T = \frac{\kappa c_0}{\gamma_0}. \tag{2}$$

Eq. (1) is a truncated expansion that also covers the case of non-spherical interfaces. It can also be noticed that the correction (1) to the surface tension transforms the surface energy into the Canham-Helfrich Hamiltonian so successfully employed in modelling biological membranes. To obtain more tractable expressions for the curvature corrections, an alternative procedure was recently put forward in Ref. [6] by performing a curvature expansion of the lowest order equation in the Born-Green-Yvon hierarchy.

Up to this point we have considered interfaces separating two distinct phases. However, *contact lines* where *three* different phases coexist at equilibrium also occur. A line energy proportional to the length of the contact curve had been introduced by Gibbs himself in [1] to model the excess free energy residing there. The constant of proportionality is called the *line tension*. Since line tension effects on equilibrium are detectable for systems in the submicrons regime, its rôle has been neglected, until exprerimental techniques became available, which allow explorations of these small-sized droplets. As a consequence, the impact of line tension on the equilibrium [7, 8] and the stability [9]-[16] of sessile droplets was studied thoroughly during the past decade. In particular, a controversy arose on the admissibility of a negative line tension within a continuum model. At variance with surface tension, Gibbs did not put restrictions on the sign of line tension, but it was proved in [9] that negative values of line tension would make the free-energy functional unbounded from below, and so make any equilibrium configuration unstable. Precisely, if the contact line is corrugated enough, a droplet at equilibrium can follow a path along which its energy is reduced. It was pointed out [12, 16, 17], however, that the characteristic wavelength induced by destabilizing perturbations on the equilibrium droplet could be a molecular length, detectable at a length-scale outside the realm of a continuum model. In [17, 18] a criterion of *marginal stability* was proposed to estimate, roughly speaking, the number of stable modes for a given equilibrium configuration and

for a given negative line tension. In this way, we could ascertain that negative line tensions as those reported in [19] were compatible with a large set of stable modes, and that the onset of instability was related to perturbations with so short a wavelength that they presumably operate at a scale where also curvature corrections to the line tension should be accounted for [17]. Incorporating these corrections into a continuum model to study their impact on the stability of sessile droplets is the aim of this paper.

In fact Boruvka and Neumann introduced long ago [20] curvature corrections for both the surface and the line energy, by building a formal theory where the free-energy contains contributions depending on both the normal and the geodesic curvatures as well as on the geodesic torsion of the contact line, conceived as a curve lying either on the substrate or on the free surface of the liquid droplet. Here we do not insist in making all these differential-geometric properties enter the free-energy functional, as this would lead to a large number of constitutive parameters which, in turn, would make predictions rather difficult, if possible at all. So, we simply imagine that the line tension depends on the curvature σ of the contact line. In this sense our approach departs from Boruvka and Neumann's who did not consider corrections only depending on the curvature σ of the contact line since σ has no relation with either the free surface of the droplet or the substrate. However, on computing the first and the second variation of the line free energy, we will see that it is natural to consider deformations of a sessile droplet that map contact lines into contact lines. In this way, the geometry of the substrate is naturally coupled with that of the contact line and both the first and the second variation of the line energy depend on the geometric properties of the contact line, conceived as a curve on the substrate.

It should also be recalled that recent studies [21] have focussed on the dependence of line tension upon the radius of curvature of the dividing line. We also mention that a different kind of curvature correction to line tension was studied in [22], where the dependence of line tension on the substrate's curvature was examined within an effective interfacial Hamiltonian approach, in the limit of weakly curved cylindric substrates.

The reader might wonder why we do not treat line and surface tension on the same footing, by assuming a dependence of this latter on curvature too. While in the next section we will give a technical reason for neglecting such corrections, a simple argument can be given, by comparing the typical energy of the term $\kappa c_0 \int_{\mathcal{S}} H \mathrm{d}A$ associated with Tolman's correction with the energy $\beta \int_{\mathcal{C}} \sigma^2 \mathrm{d}\ell$ associated with the curvature correction of line tension. Taking a spherical capsule of radius R, and recalling Eq. (2), the contribution due to curvature correction of line tension prevails whenever

$$ R \ll \sqrt{\frac{\beta}{\gamma_0 \delta_T}} \ : $$

since δ_T is a molecular length, the set of values of the ratio β/γ_0 that make this inequality obeyed by micron-sized droplets is non-empty.

This paper is organized as follows. In Section 2 we introduce the curvature correction to line tension and we discuss the length-scales hidden in our model. In Section 3 we compute the first variation of the curvature correction arriving at a modified Young

equation obeyed along the contact line. Here we also write down the second variation of the curvature-dependent correction, deferring to an Appendix the lengthly calculations needed to obtain it. As an application, in Section 4 we address the stability of a liquid bridge lying on a flat substrate that was explored without curvature correction in [14] and [15]. We prove that the curvature correction cancels the systematic instability induced by negative line tension for modes with arbitrarily short wavelengths, regardless of the magnitude of the correction. However, different stability scenarios can be singled out, depending on the magnitude of both the bare line tension and its curvature correction. The paper is closed by a section where we summarize our results and we outline some possible applications.

2   Free energy

We consider a sessile droplet $\mathcal{B}$ consisting of incompressible fluid (see Figure 1). Its
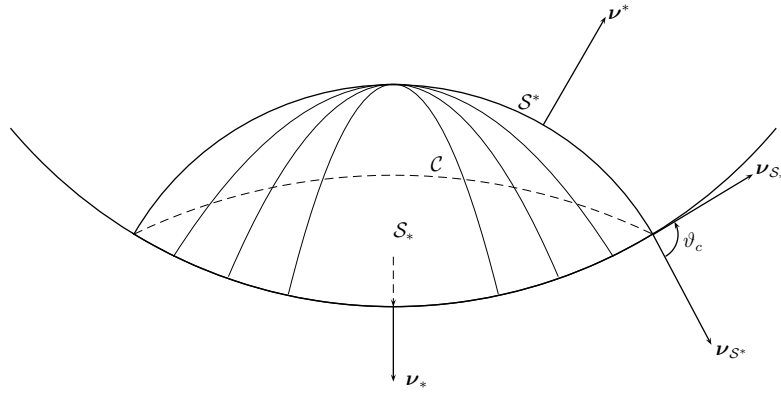
Figure 1: A sessile droplet laid on a rigid substrate. The boundary of the droplet is split into a free surface $\mathcal{S}^*$ and an adhering surface $\mathcal{S}_*$: on the former, the droplet is in contact with a vapour phase, on the latter it is in contact with the substrate. These surfaces meet along the contact line $\mathcal{C}$. The outer unit normal vectors $\boldsymbol{\nu}$ and $\boldsymbol{\nu}_*$ to $\mathcal{S}^*$ and $\mathcal{S}_*$ are also shown, together with the conormal unit vectors $\boldsymbol{\nu}_{\mathcal{S}^*}$ and $\boldsymbol{\nu}_{\mathcal{S}_*}$ to the contact line, conceived as a curve on $\mathcal{S}^*$ and $\mathcal{S}_*$, respectively. Finally, the contact angle ϑ_c, defined as the angle between $\boldsymbol{\nu}_{\mathcal{S}^*}$ and $\boldsymbol{\nu}_{\mathcal{S}_*}$, is also shown.

boundary $\partial\mathcal{B}$ is naturally split as $\partial\mathcal{B} = \mathcal{S}^* \cup \mathcal{S}_*$ where the *adhering* surface $\mathcal{S}_*$ is laid on a rigid substrate. The portion $\mathcal{S}^*$ of $\partial\mathcal{B}$ that is not in contact with the substrate is referred to as the *free* surface. The curve $\mathcal{C} := \mathcal{S}^* \cap \mathcal{S}_*$ is the *contact* line, where three phases coexist at equilibrium. We shall assume, for simplicity, that $\mathcal{C}$ is connected. The equilibrium shapes of a droplet are the critical points of the following free-energy functional

$$\mathcal{F}[\mathcal{B}] := \gamma_0 \int_{\mathcal{S}^*} \mathrm{d}a - w \int_{\mathcal{S}_*} \mathrm{d}a + \tau_0 \int_{\mathcal{C}} \mathrm{d}\ell + \beta \int_{\mathcal{C}} \sigma^2 \mathrm{d}\ell \tag{3}$$

that consists of several contributions. Firstly, $\gamma_0 \int_{\mathcal{S}^*} \mathrm{d}a$ accounts for the surface tension $\gamma_0 := \gamma_{lv} > 0$ associated with the interface between the liquid and the vapour phase. Here a is the area-measure on either $\mathcal{S}^*$ or $\mathcal{S}_*$. The term $-w \int_{\mathcal{S}_*} \mathrm{d}a$ is responsible for the excess energy at the solid-liquid interface. We introduced the *adhesion potential* $w > 0$ that is often expressed as $w = \gamma_{lv} - \gamma_{ls} + \gamma_{sv}$, where the surface tensions γ_{ls} and γ_{sv} associated with the liquid-solid and with the solid-vapour interfaces intervene. We then consider two line-energy contributions, $\tau_0 \int_{\mathcal{C}} \mathrm{d}\ell$, associated with the *bare* line tension τ_0, a constant associated with an ideal straight contact line, and $\beta \int_{\mathcal{C}} \sigma^2 \mathrm{d}\ell$, where σ is the curvature of the contact line $\mathcal{C}$ and $\beta > 0$ is a constant parameter. This term measures the curvature correction to the bare line tension and a squared dependence upon σ has been chosen because a linear term $\int_{\mathcal{C}} \sigma \mathrm{d}\ell$ would simply contribute a constant to $\mathcal{F}$, since $\mathcal{C}$ is a closed curve. Here ℓ is the length-measure along $\mathcal{C}$. In studying the impact of curvature corrections on the stability of liquid droplets, Tolman length plays an ancillary rôle. In fact, we learnt in previous work on this topic [15, 17] that the stability is determined by the natural boundary condition along the contact line that arises in the minimization of the second variation of the free-energy functional. Incorporating a curvature correction to the surface tension would add to this boundary condition terms depending on the curvature of the contact line that are qualitatively equivalent to those considered here. Moreover, this dependence would lead to a non-constant mean curvature in the free-surface profile that would render the normal mode analysis more intricate to follow. Hence, we think that the essential effects of curvature corrections are captured by just taking a curvature-dependent line tension. No bulk terms have been included in (3), thus excluding both gravitational effects, as well as the bulk terms that are introduced into effective interfacial models that bridge the continuum and the statistical approach (see, *e.g.* [23]). Since the stability of the contact line is independent of the presence of bulk terms, we think that this omission has not serious drawbacks.

We aim at exploring the stabilizing rôle of a curvature correction to the line tension and so we will assume hereafter $\tau_0 < 0$ since negative line tensions play a systematic, destabilizing effect. As we discussed in several geometries [15, 17, 18], conditionally stable equilibria in the presence of negative line tension are possible provided that $|\tau_0|$ is sufficiently small. In this case, it can be shown that the typical wavelength of destabilizing modes is a molecular length, that lies outside the realm of application of the continuum picture adopted here. We expect that a curvature correction penalizing wild oscillations of the contact line could enhance the stability of an equilibrium configuration, even if line tension is negative.

We now digress slightly to introduce the characteristic lengths hidden in our model. A first length scale ℓ_τ can be defined as the typical linear dimension of a droplet for which the surface energy and the line energy associated with bare line tension τ_0 have the same order of magnitude:

$$\gamma_0 \int_{\mathcal{S}^*} \mathrm{d}a \approx |\tau_0| \int_{\mathcal{C}} \mathrm{d}\ell \,.$$

If $\mathcal{S}^*$ is a spherical capsule of radius ℓ_τ so that $\mathcal{C}$ is a circumference of radius $R \propto \ell_\tau$, we obtain $\ell_\tau \approx |\tau_0|/\gamma_0$. Estimates for ℓ_τ can be obtained from line tension measurements

like those in [19], and range from 10^{-8} to 10^{-6} m. The following ratio

$$\xi := \frac{\tau_0}{\gamma_0} \tag{4}$$

will be employed in the application shown in Sec. 4. Finally, we can define a length ℓ_β as the typical size of a droplet for which

$$|\tau_0| \int_{\mathcal{C}} \mathrm{d}\ell \equiv \beta \int_{\mathcal{C}} \sigma^2 \mathrm{d}\ell$$

so that $\ell_\beta \approx \sqrt{\beta/|\tau_0|}$. We are unaware of any measure or estimate of ℓ_β. Although it might be reasonable to assume $\ell_\beta \ll \ell_\tau$, we will not make such a restriction in this paper. In any case, we do not need to apply our model up to the small lengths discussed here to appreciate the effects of line energies. As we will see in Sec. 4, for instance, β could affect the stability of equilibrium configurations both quantitatively and qualitatively, even if it does not modify the equilibrium profile of $\mathcal{C}$ at all.

3   Equilibrium and stability

The first and the second variation of the free-energy functional $\mathcal{F}$ in (3) have been computed in [13] for $\beta = 0$. Here we simply arrive at the first variation $\delta\mathcal{F}^*$ of the reduced functional

$$\mathcal{F}^*[\mathcal{C}] := \int_{\mathcal{C}} \sigma^2 \mathrm{d}\ell : \tag{5}$$

the equilibrium equation obeyed by the droplet $\mathcal{B}$ is obtained by adding $\beta\delta\mathcal{F}^*$ to the Young equation (Eq. $(2.44)_2$ of [13]) specialized to to case where both the surface and the bare line tension are constant. It will be useful to write the functional $\mathcal{F}$ as

$$\mathcal{F} = \mathcal{F}_0 + \beta\mathcal{F}^* \,,$$

where $\mathcal{F}_0$ is the free-energy functional when $\beta = 0$.

Since $\mathcal{F}^*$ is concentrated along the contact line, it cannot affect the equilibrium shape of the free surface $\mathcal{S}^*$ which, in the absence of bulk contributions, is a surface with constant mean curvature.

To compute $\delta\mathcal{F}^*$ we perturb $\mathcal{C}$ by mapping points $p \in \mathcal{C}$ into points

$$p \mapsto p_\varepsilon := p + \varepsilon\boldsymbol{u} + \varepsilon^2\boldsymbol{v}, \tag{6}$$

where the regular fields $\boldsymbol{u}$ and $\boldsymbol{v}$ are defined on $\mathcal{S}$. Since we do not repeat the computations for the complete functional $\mathcal{F}$, here we can deal with the restrictions of these fields along $\mathcal{C}$. In general, $\boldsymbol{u}$ and $\boldsymbol{v}$ are subject to the constraints [13]

$$\boldsymbol{u} \cdot \boldsymbol{\nu}_* = 0 \quad \text{and} \quad \boldsymbol{v} \cdot \boldsymbol{\nu}_* = -\frac{1}{2}\boldsymbol{u} \cdot (\nabla_{\mathrm{s}}\boldsymbol{\nu}_*)\boldsymbol{u} \quad \text{on } \mathcal{S}_* \tag{7}$$

where $\nabla_{\mathrm{s}}\boldsymbol{\nu}_* := (\nabla\boldsymbol{\nu}_*)(\boldsymbol{I} - \boldsymbol{\nu}_* \otimes \boldsymbol{\nu}_*)$ is the surface gradient of the outer unit normal $\boldsymbol{\nu}_*$ of $\mathcal{S}_*$. Eqs. (7) guarantee that the perturbed contact line glides on the substrate both

at the first-order—Eq. $(7)_1$—and at the second-order—Eq. $(7)_2$—in the perturbation parameter ε. The field $\boldsymbol{v}$ does not enter in the equilibrium equations, but it plays a crucial rôle in the stability of the equilibrium configurations.

Let s be the arc-length of the contact line $\mathcal{C}$, and $\boldsymbol{t}_*$ its unit-tangent vector. We will frequently use the Darboux trihedron associated with $\mathcal{C}$: it is the set $\{\boldsymbol{t}_*, \boldsymbol{\nu}_*, \boldsymbol{\nu}_{\mathcal{S}_*}\}$ formed by three orthogonal unit vectors: $\boldsymbol{t}_*$, $\boldsymbol{\nu}_*$ and $\boldsymbol{\nu}_{\mathcal{S}_*} := \boldsymbol{t}_* \wedge \boldsymbol{\nu}_*$, the *conormal* unit vector of $\mathcal{C}$ on $\mathcal{S}_*$. When a point moves along $\mathcal{C}$, the associated Darboux trihedron obeys the following Darboux equations (*see* p.241 of [24])

$$\begin{cases} \dfrac{\mathrm{d}\boldsymbol{t}_*}{\mathrm{d}s} = \kappa_g^* \boldsymbol{\nu}_{\mathcal{S}_*} + \kappa_n^* \boldsymbol{\nu}_* \\[2mm] \dfrac{\mathrm{d}\boldsymbol{\nu}_{\mathcal{S}_*}}{\mathrm{d}s} = -\kappa_g^* \boldsymbol{t}_* - \tau_g^* \boldsymbol{\nu}_* \\[2mm] \dfrac{\mathrm{d}\boldsymbol{\nu}_*}{\mathrm{d}s} = -\kappa_n^* \boldsymbol{t}_* + \tau_g^* \boldsymbol{\nu}_{\mathcal{S}_*} \,, \end{cases} \tag{8}$$

where

$$\kappa_n^* := \frac{\mathrm{d}\boldsymbol{t}^*}{\mathrm{d}s} \cdot \boldsymbol{\nu}_*, \quad \kappa_g^* := \frac{\mathrm{d}\boldsymbol{t}^*}{\mathrm{d}s} \cdot \boldsymbol{\nu}_{\mathcal{S}_*}, \quad \text{and} \quad \tau_g^* := \frac{\mathrm{d}\boldsymbol{\nu}_*}{\mathrm{d}s} \cdot \boldsymbol{\nu}_{\mathcal{S}_*} \tag{9}$$

are, respectively, the *normal curvature*, the *geodesic curvature*, and the *geodesic torsion* of $\mathcal{C}$, viewed as a curve on the substrate $\mathcal{S}_*$. Hereafter, to avoid clutter, we keep the star * only when we are referring to the unit normal $\boldsymbol{\nu}_*$ of $\mathcal{S}_*$, and when confusion might occur. No ambiguity should arise, since we always imagine $\mathcal{C}$ as a curve on $\mathcal{S}_*$.

By Eq. (6), we obtain

$$\frac{\mathrm{d}p_\varepsilon}{\mathrm{d}s} = \boldsymbol{t} + \varepsilon \boldsymbol{u}' + \varepsilon^2 \boldsymbol{v}'$$

and so

$$\frac{\mathrm{d}s}{\mathrm{d}s_\varepsilon} = \left| \frac{\mathrm{d}p_\varepsilon}{\mathrm{d}s} \right|^{-1} = [1 + 2\varepsilon \boldsymbol{u} \cdot \boldsymbol{t} + \varepsilon^2 (\boldsymbol{u}' \cdot \boldsymbol{u}' + 2\boldsymbol{v}' \cdot \boldsymbol{t})]^{-1/2} \,,$$

where a prime denotes differentiation with respect to s. Since

$$\boldsymbol{t}_\varepsilon = \frac{\mathrm{d}p_\varepsilon}{\mathrm{d}s_\varepsilon} = \frac{\mathrm{d}p_\varepsilon}{\mathrm{d}s} \frac{\mathrm{d}s}{\mathrm{d}s_\varepsilon} \,,$$

it follows that

$$\boldsymbol{t}_\varepsilon = \boldsymbol{t} + \varepsilon[\boldsymbol{u}' - (\boldsymbol{u}' \cdot \boldsymbol{t})\boldsymbol{t}] + \varepsilon^2 [\boldsymbol{v}' - \frac{1}{2}(\boldsymbol{u}' \cdot \boldsymbol{u}')\boldsymbol{t} - (\boldsymbol{v}' \cdot \boldsymbol{t})\boldsymbol{t} + \frac{3}{2}(\boldsymbol{u}' \cdot \boldsymbol{t})^2 \boldsymbol{t} - (\boldsymbol{u}' \cdot \boldsymbol{t})\boldsymbol{u}'] + O(\varepsilon^3) \,.$$

We introduce the vector fields

$$\boldsymbol{a} := \boldsymbol{u}' - (\boldsymbol{u}' \cdot \boldsymbol{t})\boldsymbol{t} \quad \text{and} \quad \boldsymbol{c} := \boldsymbol{v}' - (\boldsymbol{v}' \cdot \boldsymbol{t})\boldsymbol{t} \tag{10}$$

that satisfy $\boldsymbol{a} \cdot \boldsymbol{t} = \boldsymbol{c} \cdot \boldsymbol{t} = 0$. By setting $a^2 := \boldsymbol{a} \cdot \boldsymbol{a}$, we have $\boldsymbol{u}' \cdot \boldsymbol{u}' = a^2 + (\boldsymbol{u}' \cdot \boldsymbol{t})^2$ and so we can recast $\boldsymbol{t}_\varepsilon$ as

$$\boldsymbol{t}_\varepsilon = \boldsymbol{t} + \varepsilon \boldsymbol{a} + \varepsilon^2 [\boldsymbol{c} - \frac{a^2}{2}\boldsymbol{t} - (\boldsymbol{u}' \cdot \boldsymbol{t})\boldsymbol{a}] + O(\varepsilon^3) \,. \tag{11}$$

7

For a regular curve, the first Frénet-Serret equation states that

$$\frac{\mathrm{d}\boldsymbol{t}}{\mathrm{d}s} = \sigma\boldsymbol{n} \tag{12}$$

where $\boldsymbol{n}$ is the principal unit normal to the curve. Hence, on $\mathcal{C}_\varepsilon$ we have

$$\sigma_\varepsilon = \left[\frac{\mathrm{d}\boldsymbol{t}_\varepsilon}{\mathrm{d}s_\varepsilon} \cdot \frac{\mathrm{d}\boldsymbol{t}_\varepsilon}{\mathrm{d}s_\varepsilon}\right]^{1/2}$$

which, after rearrangements yields

$$\sigma_\varepsilon^2 \frac{\mathrm{d}s_\varepsilon}{\mathrm{d}s} = \frac{\mathrm{d}\boldsymbol{t}_\varepsilon}{\mathrm{d}s} \cdot \frac{\mathrm{d}\boldsymbol{t}_\varepsilon}{\mathrm{d}s}\frac{\mathrm{d}s}{\mathrm{d}s_\varepsilon}. \tag{13}$$

By use of Eqs. (11) and (12) and after tedious but straightforward computations we obtain

$$\sigma_\varepsilon^2 \tfrac{\mathrm{d}s_\varepsilon}{\mathrm{d}s} = \sigma^2 + \varepsilon[2\sigma\boldsymbol{a}' \cdot \boldsymbol{n} - \sigma^2(\boldsymbol{u}' \cdot \boldsymbol{t})] + \varepsilon^2[\boldsymbol{a}' \cdot \boldsymbol{a}' + 2\sigma\boldsymbol{n} \cdot \boldsymbol{c}' -$$
$$-2\sigma(\boldsymbol{u}' \cdot \boldsymbol{t})'\boldsymbol{n} \cdot \boldsymbol{a} - 4\sigma(\boldsymbol{u}' \cdot \boldsymbol{t})\boldsymbol{n} \cdot \boldsymbol{a}' - \tfrac{3}{2}a^2\sigma^2 + \sigma^2(\boldsymbol{u}' \cdot \boldsymbol{t})^2 - \sigma^2\boldsymbol{v}' \cdot \boldsymbol{t}]. \tag{14}$$

By definition, the first variation $\delta\mathcal{F}^*$ of $\mathcal{F}^*$ is given by

$$\delta\mathcal{F}^* := \left.\frac{\mathrm{d}\mathcal{F}^*[\mathcal{C}_\varepsilon]}{\mathrm{d}\varepsilon}\right|_{\varepsilon=0} = \int_\mathcal{C}[2\sigma\boldsymbol{a}' \cdot \boldsymbol{n} - \sigma^2(\boldsymbol{u}' \cdot \boldsymbol{t})]\mathrm{d}s = \int_\mathcal{C}[(\sigma^2\boldsymbol{t})' \cdot \boldsymbol{u} - 2(\sigma\boldsymbol{n})' \cdot \boldsymbol{a}]\mathrm{d}s \tag{15}$$

where integration by parts has been used in the last passage. By recalling the definition of $\boldsymbol{a}$ in Eq. (10) and by performing several integrations by parts to get rid of the derivatives $\boldsymbol{u}'$, we obtain

$$\delta\mathcal{F}^* = \int_\mathcal{C}\{[(\sigma^2\boldsymbol{t})' + 2(\sigma\boldsymbol{n})'' - 2[((\sigma\boldsymbol{n})' \cdot \boldsymbol{t})\boldsymbol{t}]'\} \cdot \boldsymbol{u}\mathrm{d}s.$$

Since the second Frénet-Serret equation reads

$$\frac{\mathrm{d}\boldsymbol{n}}{\mathrm{d}s} = -(\sigma\boldsymbol{t} + \widetilde{\tau}\boldsymbol{b}),$$

where $\widetilde{\tau}$ and $\boldsymbol{b} := \boldsymbol{t} \wedge \boldsymbol{n}$ are the torsion and the unit binormal vector of $\mathcal{C}$, we finally arrive at

$$\delta\mathcal{F}^* = \int_\mathcal{C}\boldsymbol{u} \cdot [3(\sigma^2\boldsymbol{t})' + 2(\sigma\boldsymbol{n})'']\mathrm{d}s.$$

The differential properties of $\mathcal{C}$ as a curve on $\mathcal{S}_*$ enter the scene when Eq. $(8)_1$ is compared with Eq. (12) so that $\delta\mathcal{F}^*$ reads as

$$\delta\mathcal{F}^* = \int_\mathcal{C}\boldsymbol{u} \cdot [6\sigma\sigma'\boldsymbol{t} + 3\sigma^3\boldsymbol{n} + 2(\kappa_g\boldsymbol{\nu}_\mathcal{S} + \kappa_n\boldsymbol{\nu}_*)'']\mathrm{d}s.$$

8

Since, by Eq. $(7)_1$,

$$\boldsymbol{u} = u_t \boldsymbol{t} + u_s \boldsymbol{\nu}_{\mathcal{S}} \tag{16}$$

along $\mathcal{C}$, by applying repeatedly Darboux equations (8), by performing several integrations by parts and by using the identity

$$\sigma^2 = \kappa_g^2 + \kappa_n^2 \,, \tag{17}$$

we obtain

$$\delta\mathcal{F}^* = \int_{\mathcal{C}}\{[\kappa_g\sigma^2 + 2(\tau_g'\kappa_n + 2\tau_g\kappa_n' + \kappa_g'' - \kappa_g\tau_g^2)]u_s +$$

$$+2[\sigma\sigma' - \kappa_g\kappa_g' - \kappa_n\kappa_n']u_t\}\mathrm{d}s = \int_{\mathcal{C}}[\kappa_g\sigma^2 + 2(\tau_g'\kappa_n + 2\tau_g\kappa_n' + \kappa_g'' - \kappa_g\tau_g^2)]u_s\mathrm{d}s \,,$$

where Eq. (17) was differentiated with respect to s to suppress the term multiplying u_t. The first variation $\delta\mathcal{F}^*$ is thus independent of the component u_t of $\boldsymbol{u}$ along the unit tangent vector $\boldsymbol{t}$ of $\mathcal{C}$, as it should be, since u_t simply reparameterizes $\mathcal{C}$. One could assume a pragmatic attitude by setting $u_t \equiv 0$ from the very beginning. We prefer to keep this term since its disappearance from both the first and the second variation serves as a check of consistency for our computations.

If $\beta\delta\mathcal{F}^*$ is added to the first variation of $\mathcal{F}_0$ as given in Eq. (2.44) of [13], the following equilibrium equation should be obeyed along $\mathcal{C}$

$$\gamma_0\cos\vartheta_c + \gamma_0 - w - \tau_0\kappa_g + \beta\kappa_g\sigma^2 + 2\beta(\tau_g'\kappa_n + 2\tau_g\kappa_n' + \kappa_g'' - \kappa_g\tau_g^2) = 0 \,, \tag{18}$$

where ϑ_c is the *contact angle*, that is, the angle between the conormal unit vectors $\boldsymbol{\nu}_{\mathcal{S}^*}$ and $\boldsymbol{\nu}_{\mathcal{S}_*}$ of $\mathcal{C}$ viewed as a curve on either $\mathcal{S}^*$ or $\mathcal{S}_*$, respectively (see Fig. 1). At variance with Eq. (2.44) of [13], the subscript $_*$ has been dropped since no confusion can arise here.

The format just employed gives also the second variation of $\mathcal{F}^*$. Since computations are much more involved, however, we prefer to move the details into an Appendix, while here we simply record the final result:

$$\delta^2\mathcal{F}^* = \int_{\mathcal{C}}(u_s'')^2\mathrm{d}s + \int_{\mathcal{C}}(6\tau_g^2 - \kappa_g^2 - \tfrac{3}{2}\sigma^2)(u_s')^2\mathrm{d}s + \int_{\mathcal{C}}\{\tau_g^4 + (\tau_g')^2 + \sigma^2(\kappa_g^2 - \tfrac{3}{2}\tau_g^2) +$$

$$+(\kappa_n\tau_g)^2 + 2\kappa_n\kappa_g'\tau_g - 4\tau_g^2\kappa_g^2 + 4\kappa_g\tau_g\kappa_n' + [2\tau_g\kappa_g\kappa_n + 3\kappa_g\kappa_g']' +$$

$$+(H - \kappa_n)(\tfrac{1}{2}\sigma^2\kappa_n + \kappa_n'' - 2\tau_g\kappa_g' - \kappa_g\tau_g' - \kappa_n\tau_g^2)\}u_s^2\mathrm{d}s \,, \tag{19}$$

where H is the total curvature of $\mathcal{S}_*$. By adding $\beta\delta^2\mathcal{F}^*$ to Eq. (3.16) of [13] we obtain the complete second variation of the functional $\mathcal{F}$. We remind the reader that u_{s*} in [13] coincides with u_s employed here.
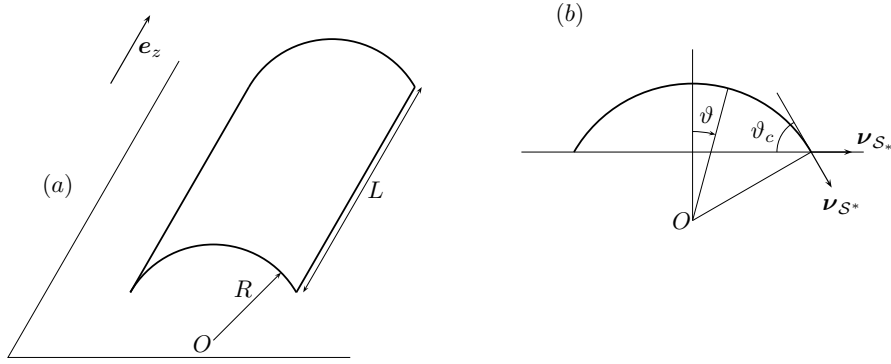
Figure 2: a): Sketch of a liquid bridge, conceived as a straight circular cylinder of radius R, with symmetry axis along $\boldsymbol{e}_z$. The bridge is laid on a flat substrate. Here L denotes the typical length along which the cylinder is perturbed. b) the cylindric polar coordinates z and ϑ used to parameterize the free surface of the bridge are shown together with the contact angle ϑ_c, which is constant along the contact line. The conormal unit vectors $\boldsymbol{\nu}_{\mathcal{S}^*}$ and $\boldsymbol{\nu}_{\mathcal{S}_*}$ of $\mathcal{C}$ as a curve on either the free or the adhering surface of the bridge have been drawn too.

4 Application

We apply the results of the previous sections to study the stability of a liquid bridge, conceived as a straight circular cylinder with radius R laid on a flat substrate (see Figure 2a). Since a cylinder is a surface with constant mean curvature, it represents an admissible equilibrium free surface. By Eq. (18), we see that a straight equilibrium contact line is unaffected by both the line tension and its curvature correction: the contact angle has a constant value ϑ_c along $\mathcal{C}$. We assume that the cylinder's axis lies along the $\boldsymbol{e}_z$ direction and we parameterize the free surface of the cylinder by using the angle $\vartheta \in [-\vartheta_c, \vartheta_c]$ and $z \in \mathbb{R}$ (see Fig. 2b). Since $\sigma = \kappa_n = \kappa_g = \tau_g = 0$, by Eq. (19) we have

$$\beta \delta^2 \mathcal{F}^* = \beta \int_{\mathcal{C}} (u_s'')^2 \mathrm{d}s$$

that, when added to the second variation of $\mathcal{F}_0$ (see Eq. (3) of [15])

$$\delta^2 \mathcal{F}_0[\boldsymbol{u}] = \gamma_0 \int_{\mathcal{S}^*} \left\{ |\nabla_{\mathrm{s}} u_\nu|^2 - \frac{1}{R^2} u_\nu^2 \right\} \mathrm{d}a + \int_{\mathcal{C}} \left\{ \tau_0 (u_s')^2 - \frac{\gamma_0}{R} \cos \vartheta_c \sin \vartheta_c u_s^2 \right\} \mathrm{d}s \,,$$

yields the second variation of the functional $\mathcal{F}$

$$\delta^2 \mathcal{F}[\boldsymbol{u}] = \gamma_0 \int_{\mathcal{S}^*} \left\{ |\nabla_{\mathrm{s}} u_\nu|^2 - \frac{1}{R^2} u_\nu^2 \right\} \mathrm{d}a + \int_{\mathcal{C}} \left\{ \beta (u_s'')^2 + \tau_0 (u_s')^2 - \frac{\gamma_0}{R} \cos \vartheta_c \sin \vartheta_c u_s^2 \right\} \mathrm{d}s \,.$$
(20)

In eq. (20), $\nabla_{\mathrm{s}} u_\nu = (\boldsymbol{I} - \boldsymbol{\nu} \otimes \boldsymbol{\nu}) \nabla u_\nu$ is the surface gradient of the scalar field u_ν. We warn the reader that in [15] the line tension was denoted by γ, and the surface tension

10

by τ. In Eq. (20), u_ν is the component of $\boldsymbol{u}$ along the outer unit normal vector of the free surface $\mathcal{S}^*$ and it is related to u_s via the equation

$$u_\nu = \sin\vartheta_c u_s \,. \tag{21}$$

With the aid of Eq. (21), $\delta^2\mathcal{F}$ becomes a quadratic functional of u_ν and so, either its minimum is zero, or it is unbounded from below. To deal with finite minima, we minimize $\delta^2\mathcal{F}$ on the set of functions obeying the constraint

$$\int_{\mathcal{S}^*} u_\nu^2 \mathrm{d}a = 1 \ : \tag{22}$$

if the minimum of $\delta^2\mathcal{F}$ on this set is positive, $\delta^2\mathcal{F}$ is positive definite, and so the equilibrium configuration is locally stable whereas, if the minimum of $\delta^2\mathcal{F}$ on the set (22) is negative, the equilibrium configuration is unstable [13]. Since we assume that the liquid bridge is made of incompressible fluid, u_ν should also obey the incompressibility constraint

$$\int_{\mathcal{S}^*} u_\nu \mathrm{d}a \,. \tag{23}$$

The constraint (23), together with its second order implementation (Eq. $(2.29)_2$ of [13]) have been used in [13, 15] to obtain both the first and the second variation of $\mathcal{F}_0$. Until now we did not need them since we only dealt with $\mathcal{F}^*$ which is unaffected by this constraint, as it is concentrated on $\mathcal{C}$. However, to proceed we need to study $\delta^2\mathcal{F}$ and so we have to enforce incompressibility as well. Precisely, the first-order requirement (23) is needed since we have to compute only the first variation of $\delta^2\mathcal{F}$. Hence, we minimize the quadratic functional

$$\mathcal{G}[u_\nu] := \delta^2\mathcal{F}[u_\nu] - \frac{\mu}{2}\int_{\mathcal{S}} u_\nu^2 \mathrm{d}a + \lambda\int_{\mathcal{S}^*} u_\nu \mathrm{d}a \,,$$

where $\mu/2$ and λ are Lagrange multipliers corresponding to the constraints (22) and (23). The scalar field u_ν is perturbed according to

$$u_\nu \mapsto u_{\nu\varepsilon} := u_\nu + \varepsilon\, h \,,$$

where h is a regular scalar field. Here we focus on the contribution arising from curvature correction. Much in the spirit of Rayleigh instability, we imagine that the cylinder has infinite length and we call L the length of $\mathcal{C}$ over which perturbations are effective. As a consequence, we require

$$u_\nu(\vartheta, 0) = u_\nu(\vartheta, L) = 0\,, \qquad \forall\vartheta \in [-\vartheta_c, \vartheta_c] \tag{24}$$

so that also h has to vanish at $z = 0, L$. By setting $\chi := 1/\sin\vartheta_c$, using Eq. (21) and integrating by parts twice, we obtain

$$\int_{\mathcal{C}} (u_{s\varepsilon}'')^2 \mathrm{d}\ell = \int_0^L (u_{s\varepsilon}'')^2 \mathrm{d}z = \chi^2 \int_0^L (u_\nu'')^2 \mathrm{d}z + 2\chi^2\int_0^L h\, u_\nu^{(\mathrm{iv})}\mathrm{d}z + u_\nu''(L)\, h'(L) - u_\nu''(0)\, h'(0)\,, \tag{25}$$

11

where a prime stands for differentiation along the arc-length z of $\mathcal{C}$, and use of Eq. (24) has been made. Since in this case $\mathcal{C}$ is an open curve we need to require

$$u_\nu''(\vartheta, 0) = u_\nu''(\vartheta, L) \qquad \forall \vartheta \in [-\vartheta_c, \vartheta_c] \, . \tag{26}$$

By adding (25) to the terms of the first variation of $\mathcal{G}$ that were computed in Eqs. (7)-(8) of [15], we conclude that finding the minimum of $\mathcal{G}$ on the set (22) amounts at finding the minimum eigenvalue μ of the following problem

$$\triangle_{\mathrm{s}} u_\nu + (\mu + \frac{1}{R^2})u_\nu + \lambda \;\; = \;\; 0 \quad \text{on } \mathcal{S}^*, \tag{27}$$

$$\sin^2 \vartheta_c \nabla_{\mathrm{s}} u_\nu \cdot \boldsymbol{\nu}_\mathcal{S} + \frac{\beta}{\gamma_0} u_\nu^{(\mathrm{iv})} - \xi u_\nu'' - \frac{1}{R} \sin \vartheta_c \cos \vartheta_c u_\nu \;\; = \;\; 0 \quad \text{along } \mathcal{C} \, . \tag{28}$$

Here $\triangle_{\mathrm{s}}$ is the surface-Laplacian defined on $\mathcal{S}$ and ξ is defined according to Eq. (4). Hereafter we drop the subscript ν from u_ν. As proved in [13], the smallest value μ_{min} of μ that solves the problem (27-28) coincides with the minimum value of $\delta^2 \mathcal{F}$ on the constraint (22) and so we conclude that an equilibrium configuration is locally stable or not according to whether μ_{min} is positive or not.

To analyse Eqs. (27-28), we expand u as a sine series

$$u(\vartheta, z) = \sum_{n=1}^{\infty} a_n \sin\left(\frac{2n\pi}{L} z\right) u_n(\vartheta) \, , \tag{29}$$

where $u_n(\vartheta)$ are unknown functions of ϑ. In this class, we can satisfy the boundary conditions (24) and (26) as well as the incompressibility constraint (23), so that we can set $\lambda = 0$ in (27). The reader might wonder whether the second variation just obtained, as well as that computed in Refs. [13, 15] for sessile droplets with *closed* contact line are valid here, where the contact line is open. A glance at the derivations of the second variation in the Appendix and in Refs. [13, 15] shows that terms at the end-points of the contact line are *always* coupled with the curvature—normal or geodesic— or to the geodesic torsion of $\mathcal{C}$ which vanish identically along a straight contact line and so never contribute.

We split our discussion into two parts, according to whether $u_n(\vartheta)$ is symmetric with respect to the plane $\vartheta = 0$, or if it is skew-symmetric. We call *peristaltic* modes those in the former class, for which

$$\left.\frac{\partial u_n}{\partial \vartheta}\right|_{\vartheta=0} = 0 \quad \forall z \in [0, L] \tag{30}$$

holds and we call *varicose* the modes in the latter class, which in turn obey

$$u_n(\vartheta) = 0 \quad \forall z \in [0, L] \, . \tag{31}$$

12

4.1 Peristaltic Modes

When a mode

$$u(\vartheta, z) = \sin\left(\frac{2n\pi}{L}z\right)u_n(\vartheta) \tag{32}$$

in the expansion (29) is inserted into Eq. (27) with $\lambda = 0$ and the multiplier μ is scaled to R^2, $u_n(\vartheta)$ has to satisfy

$$\frac{1}{R^2}\ddot{u}_n - \left(\frac{2n\pi}{L}\right)^2 u_n + \left(\frac{\mu+1}{R^2}\right)u_n = 0\,,$$

where we exploited the expression

$$\triangle_{\mathrm{s}}f = \frac{1}{R^2}\frac{\partial^2 f}{\partial \vartheta^2} + \frac{\partial^2 f}{\partial z^2}$$

of the surface-Laplacian acting on a scalar function $f = f(\vartheta, z)$ defined on $\mathcal{S}^*$ and where a superimposed dot denotes differentiation with respect to ϑ. By introducing the dimensionless ratio

$$\varrho_n := \left(\frac{2\pi n R}{L}\right)^2 \tag{33}$$

and setting

$$\sigma_n := \mu + 1 - \varrho_n\,, \tag{34}$$

by Eq. (30) the peristaltic modes are given by

$$u_n(\vartheta) = \begin{cases} A\cos(\sqrt{\sigma_n}\vartheta) & \text{if } \sigma_n > 0 \\ A & \text{if } \sigma_n = 0 \\ A\cosh(\sqrt{-\sigma_n}\vartheta) & \text{if } \sigma_n < 0\,, \end{cases} \tag{35}$$

where A is an inessential constant that can be adjusted by imposing the constraint (22). If the mode (32) is inserted into Eq. (28), also by use of Eq. (35), we conclude that $u(\vartheta, z)$ is an acceptable eigenfunction if

$$\frac{\beta}{\gamma_0}\left(\frac{2n\pi}{L}\right)^4 u_n(\vartheta_c) + \frac{1}{R}\dot{u}_n(\vartheta_c) + \xi\left(\frac{2n\pi}{L}\right)^2 \varrho_n u_n(\vartheta_c) - \frac{1}{R}u_n(\vartheta_c)\sin\vartheta_c\cos\vartheta_c = 0 \tag{36}$$

holds, where we noted that

$$\nabla_{\mathrm{s}}u \cdot \boldsymbol{\nu}_{\mathcal{S}} = \frac{\partial u}{\partial \vartheta} = \dot{u}(\vartheta)\,.$$

Also by use of Eq. (4) we introduce the dimensionless parameters

$$\varepsilon := \frac{\xi}{R} = \frac{\tau_0}{\gamma_0 R} \qquad \text{and} \qquad \eta := \frac{\beta}{\gamma_0 R^3}\,.$$

By setting

$$x_n := \begin{cases} \sqrt{\sigma_n}\vartheta_c & \text{if } \sigma_n > 0 \\ \sqrt{-\sigma_n}\vartheta_c & \text{if } \sigma_n < 0\,, \end{cases} \tag{37}$$

13

we can recast (36) as

$$\eta \varrho_n^2 + \varepsilon \varrho_n = \sin \vartheta_c [\cos \vartheta_c + \frac{\sin \vartheta_c}{\vartheta_c} x_n \tan x_n] \quad \text{if } \sigma_n > 0, \tag{38}$$

$$\eta \varrho_n^2 + \varepsilon \varrho_n = \sin \vartheta_c [\cos \vartheta_c - \frac{\sin \vartheta_c}{\vartheta_c} x_n \tanh x_n] \quad \text{if } \sigma_n < 0, \tag{39}$$

and

$$\eta \varrho_n^2 + \varepsilon \varrho_n = \sin \vartheta_c \cos \vartheta_c \quad \text{if } \sigma_n = 0. \tag{40}$$

Following [15], modes satisfying (38), (39), and (40) are called *circular*, *hyperbolic*, and *linear* modes, respectively. Compared to the analysis performed in [15], the left-hand side of Eqs. (38-40) is a second- instead of a first-degree polynomial in ϱ_n: in this sense, the curvature correction acts as a singular perturbation term. As we remarked before, stable modes correspond to positive values of μ, whereas unstable modes correspond to $\mu < 0$. To ascertain the stability of a particular mode, it is then crucial to localize the marginal modes, corresponding to $\mu = 0$. By the definitions (34) and (37) we can write

$$\mu = \begin{cases} \varrho_n - 1 + \left(\frac{x_n}{\vartheta_c}\right)^2 & \text{if } \sigma_n > 0 \\ \varrho_n - 1 - \left(\frac{x_n}{\vartheta_c}\right)^2 & \text{if } \sigma_n < 0 \\ \varrho_n - 1 & \text{if } \sigma_n = 0. \end{cases} \tag{41}$$

From $(41)_1$ we conclude that points in the quadrant $\mathcal{Q} := \{(x_n, \varrho_n) | \ x_n \geq 0, \quad \varrho_n \geq 0\}$ of the (x_n, ϱ_n)-plane that lie below the parabola

$$\varrho_n = 1 - \left(\frac{x_n}{\vartheta_c}\right)^2 \tag{42}$$

are unstable against circular modes, whereas points in $\mathcal{Q}$ above this parabola are stable against circular modes. Similarly, it follows from $(41)_2$ that points of $\mathcal{Q}$ below the parabola

$$\varrho_n = 1 + \left(\frac{x_n}{\vartheta_c}\right)^2 \tag{43}$$

are unstable against hyperbolic modes, whereas points above it are stable against hyperbolic modes. Finally, points in $\mathcal{Q}$ that lie below the straight line

$$\varrho_n = 1 \tag{44}$$

are unstable against linear modes, while points above this line are stable. We now replace ϱ_n in Eqs. (38-40) with the appropriate expressions found in Eqs. (42-44), we divide Eqs. (38-40) by ε and define the functions

$$g_c(x_n) := \phi \left\{ \eta \left[1 - \left(\frac{x_n}{\vartheta_c}\right)^2 \right]^2 - \sin \vartheta_c [\cos \vartheta_c + \frac{\sin \vartheta_c}{\vartheta_c} x_n \tan x_n] \right\},$$

14

$$g_h(x_n) := \phi \left\{ \eta \left[1 + \left(\frac{x_n}{\vartheta_c} \right)^2 \right]^2 - \sin \vartheta_c [\cos \vartheta_c - \frac{\sin \vartheta_c}{\vartheta_c} x_n \tanh x_n] \right\},$$

and

$$g_l(x_n) := \phi [\eta - \sin \vartheta_c \cos \vartheta_c].$$

where, for simplicity, we set $\phi := 1/|\varepsilon|$. Increasing values of ϕ correspond to line tensions with decreasing magnitude. By Eq. (41), the marginal modes are the smaller pairs (x_n, ϱ_n) in $\mathcal{Q}$ that obey the equation

$$
\begin{cases}
1 - \left(\frac{x_n}{\vartheta_c} \right)^2 = g_c(x_n) & \text{if } \sigma_n > 0 \\
1 + \left(\frac{x_n}{\vartheta_c} \right)^2 = g_h(x_n) & \text{if } \sigma_n < 0 \\
1 = g_l(x_n) & \text{if } \sigma_n = 0
\end{cases}
\tag{45}
$$

The pairs (ϕ, ϱ_n) that solve Eq. (45) and yield the most restrictive stability condition lie on the *marginal* curve which divides the (ϕ, ϱ_n)-plane into a stable and an unstable set. Figure 3 shows the marginal curves for $\vartheta_c = 65°$ and for several values of η: no qualitative differences occur if other values of $\vartheta_c < \pi/2$ are chosen. To follow the discussion the reader is also urged to look at Fig. 4, where the semi-logarithmic plot of the marginal curves of Fig. 3 are shown. The numerical solution of Eq. (45) (and of Eq. (46) below) has been performed in a MATLAB environment by resorting to a simple bisection algorithm. An educated guess based on an *a priori* analytical study of the equation has been used to select the intervals in which the solutions are first sought. We stress that, by definition of ϕ and since we only consider negative line tensions, moving from left to right amounts at spanning the interval $(-\infty, 0)$ for the line tension.

Hyperbolic modes are most effective and, depending on the value of η, we can single out three stability diagrams, according to the profile of the marginal curve. If $\eta = 0$ (solid line a) the marginal curve has a turning point and the stability diagram coincides with that obtained in [15]. A straight line $\phi = \phi_0 = $ const. either intersects the marginal curve twice or it does not intersect it at all, according to the value of ϕ_0. When two intersections $(\phi_0, \varrho_n^{(1)})$ and $(\phi_0, \varrho_n^{(2)})$ exist $(\varrho_n^{(1)} < \varrho_n^{(2)})$, Rayleigh instability makes liquid bridges unstable when $\varrho_n < \varrho_n^{(1)}$. When $\varrho_n \in (\varrho_n^{(1)}, \varrho_n^{(2)})$ liquid bridges are locally stable and they become unstable again when $\varrho_n > \varrho_n^{(2)}$. Since ϱ_n is proportional to n, modes with $n = 1$ are more likely to induce Rayleigh instability: in fact, we leave the unstable set $\varrho_n < \varrho_n^{(1)}$ earlier and earlier on increasing n at fixed L and R. The effects of line tension are more related to the unstable set $\varrho_n > \varrho_n^{(2)}$. In this case, modes with large n are most likely to cause instability. However [15], n cannot be increased arbitrarily in a coherent theory since the typical length scale L/n associated with the corrugations induced on the contact line by the perturbation falls *below* the smallest scale that can be reached within a continuum approach. Hence, only a finite number of values of n can be considered and it is clear from Figure 3 that the smaller the line tension, the more values of n will fall within the region of local stability. When $\phi = \phi_0$ does not
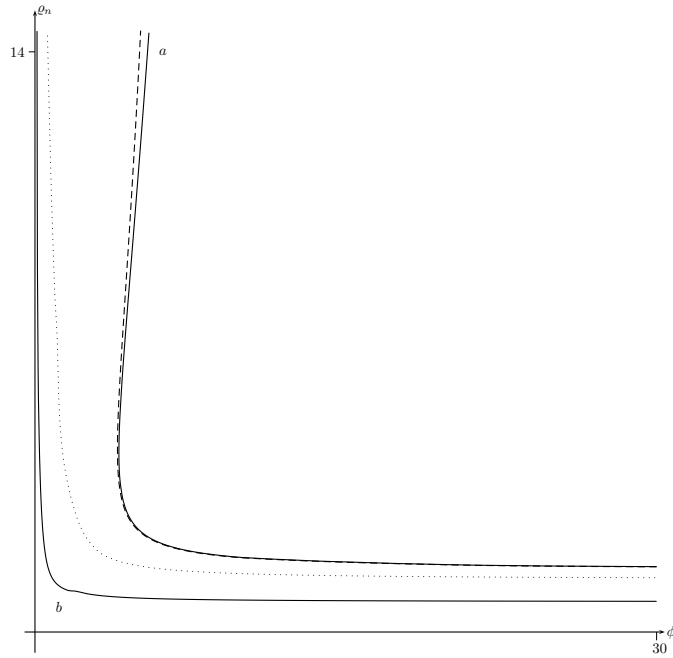
Figure 3: Stability diagram for peristaltic modes when $\vartheta_c = 65°$, for several values of η: $\eta = 0$ (solid line a), 10^{-3} (dashed line), 10^{-1} (dotted line), 1 (solid line b). Only hyperbolic modes are effective. For a given value of η, the region bounded by the coordinate axes and the marginal curve is unstable, while the remaining portion of the (ϕ, ϱ_n) plane is stable. On increasing η, Rayleigh instability persists while the instability induced by negative line tension for large values of n is reduced, since the marginal curve only diverges in the limit as $\phi \to 0$, that is, when the magnitude of line tension is exceedingly high (see also Fig. 4 for further details).

intersect the marginal curve, and so the line tension has a large magnitude, *no* stable modes survive, and no stable equilibrium liquid bridge exists.

If $\eta \in (0, \eta_c(\vartheta_c)]$ (dashed line in Fig. 3 or, better, line 2) in Fig. 4) the marginal curve has two turning points. A line $\phi = \phi_0$ crosses the marginal curve three times if $\phi_0 \in [\phi_0^m, \phi_0^M]$ and only once elsewhere. In this latter case only Rayleigh instability occurs: it is slightly reduced by a curvature correction when $\phi_0 > \phi_0^M$, but it becomes more and more restrictive if $\phi_0 < \phi_0^m$, since the marginal curve diverges along the ϱ_n axis. When $\phi_0 \in [\phi_0^m, \phi_0^M]$ the points $(\phi_0, \varrho_n^{(1)})$, $(\phi_0, \varrho_n^{(2)})$, and $(\phi_0, \varrho_n^{(3)})$ $(\varrho_n^{(1)} < \varrho_n^{(2)} < \varrho_n^{(3)})$ on the marginal curve impose the following scenario: a liquid bridge being unstable when either $\varrho_n < \varrho_n^{(1)}$ (Rayleigh instability) or $\varrho \in (\varrho_n^{(2)} < \varrho_n^{(3)})$ and stable when either $\varrho \in (\varrho_n^{(1)} < \varrho_n^{(2)})$ or $\varrho > \varrho_n^{(3)}$. In particular, the local stability when $\varrho > \varrho_n^{(3)}$ mirrors the stabilizing rôle even of a tiny curvature correction. The undulating behaviour for $\varrho_n \in (\varrho_n^{(1)}, \varrho_n^{(3)})$ disappears when η attains a critical value $\eta_c(\vartheta_c)$ at which $\phi_0^m = \phi_0^M$. For

16

larger values of η (dotted line, solid line b), Fig. 3, lines 3) and 4), Fig. 4) the marginal curve has a monotonic profile and it is crossed by a line $\phi = \phi_0$ at a unique point $(\phi_0, \varrho_n^{(1)})$: only liquid bridges such that $\varrho_n < \varrho_n^{(1)}$ are unstable: a Rayleigh instability occurs which becomes stronger and stronger when the magnitude of line tension increases. Figure 5
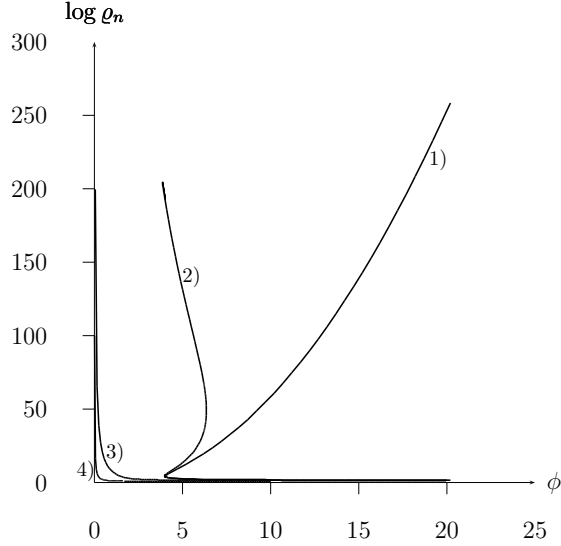
Figure 4: Semi-logarithmic plot of the stability diagram for peristaltic modes shown in Fig. 3. The four curves correspond to the values 1) $\eta = 0$, 2) $\eta = 10^{-3}$, 3) $\eta = 10^{-1}$, and 4) $\eta = 1$. The region of Rayleigh instability can be perceived only for $\eta = 10^{-1}$ and $\eta = 1$. Three regimes exist, depending on the value of η. When $\eta = 0$ a line $\phi = \phi_0$ either crosses the marginal curve twice or it does not cross it at all. This mirrors the destabilizing rôle of negative line tension when there are no curvature corrections. The second regime covers the set $\eta \in (0, \eta_c]$ (curve 2): then, when ϕ is either very small or large $\phi = \phi_0$ crosses the marginal curve only once, and so only Rayleigh instability occurs. There is an intermediate set of values of ϕ_0 for which three intersections exist between $\phi = \phi_0$ and the marginal curve. Finally, when $\eta > \eta_c$ there is always one intersection between a line $\phi = \phi_0$ and the marginal curve: only Rayleigh instability occurs here.

shows the graph of $\eta_c(\vartheta_c)$ against the contact angle ϑ_c. We conclude that small and large values of ϑ_c require lower values of η to wash out the instability at large n typical of a negative line tension. To prove that the marginal curve cannot diverge in the limit $\phi \to \infty$ and when η assumes any *fixed*, non-vanishing value, we simply look at Eqs. (45) *before* division by ε is performed. By applying the method of dominant balance [26], we conclude that $\varrho_n \to \infty$ and $\phi \to \infty$ would yield

$$\eta \varrho_n^2 = -\frac{\sin^2 \vartheta_c}{\vartheta_c} x_n \tanh x_n$$

17
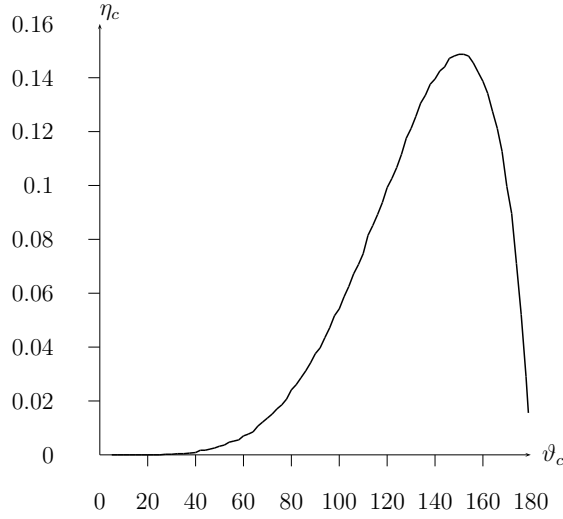
Figure 5: The critical value η_c of η is plotted against the contact angle ϑ_c for peristaltic modes. When η exceeds η_c, the marginal curve is a monotonic function of ϕ.

which is clearly inconsistent because of the different sign of the two sides. Similarly, we exclude that ϱ_n could diverge at a finite value of ϕ. Hence, given a fixed value of $\eta > 0$ ϱ_n could diverge only in the limit where $\phi \to 0$, that is, if the negative line tension has a large magnitude. This argument corroborates the outcomes of the numerical analysis of Eq. (45). Figure 6 shows the stability of a liquid bridge against peristaltic modes, when the contact angle is larger than $\pi/2$: precisely, here $\vartheta_c = 125°$. Both circular and hyperbolic modes are effective in this case but, apart from this, there is no substantial difference from the case where $\vartheta_c < \pi/2$. Similarly, the semi-logarithmic plot shown in Fig. 7 does not have new features as compared with that shown in Fig. 4.

4.2 Varicose modes

In this class, $u_n(0) \equiv 0$ and so, by retracing the same steps as before, we obtain

$$u_n = \begin{cases} A\sin(\sqrt{\sigma_n}\vartheta) & \text{if } \sigma_n > 0 \\ A\sinh(\sqrt{-\sigma_n}\vartheta) & \text{if } \sigma_n < 0 \, , \end{cases}$$

for circular and hyperbolic modes, respectively, while linear modes are absent. From this point, the analysis of Sec. 4.1 can be repeated *verbatim*. After introducing the functions

$$k_c(x_n) := \phi \left\{ \eta \left[1 - \left(\frac{x_n}{\vartheta_c} \right)^2 \right]^2 - \sin\vartheta_c [\cos\vartheta_c - \frac{\sin\vartheta_c}{\vartheta_c} x_n \cot x_n] \right\} \, ,$$

$$k_h(x_n) := \phi \left\{ \eta \left[1 + \left(\frac{x_n}{\vartheta_c} \right)^2 \right]^2 - \sin\vartheta_c [\cos\vartheta_c - \frac{\sin\vartheta_c}{\vartheta_c} x_n \coth x_n] \right\} \, ,$$

18

marginal modes are obtained by determining the smallest pairs in $\mathcal{Q}$ that obey

$$\begin{cases} 1 - \left(\frac{x_n}{\vartheta_c}\right)^2 = k_c(x_n) & \text{if } \sigma_n > 0 \\ 1 + \left(\frac{x_n}{\vartheta_c}\right)^2 = k_h(x_n) & \text{if } \sigma_n < 0\,. \end{cases} \tag{46}$$

Figure 8 shows the stability diagram of a liquid bridge against varicose modes, when $\vartheta_c = 65°$. The branch of the marginal curve corresponding to Rayleigh instability disappears. When $\phi \to \infty$, varicose modes are stable, as it should be, since they do not affect Rayleigh instability in the absence of line tension. Let us first consider the case $\eta = 0$. When the magnitude of negative line tension is progressively decreased, instability occurs for large values of ϱ_n. To grasp the behaviour of the marginal curve in the limit where $\phi \to \infty$, we still employ the method of dominant balance. Since large values of ϱ_n also imply large values of x_n by Eq. (43), we can look for solutions to Eq. $(46)_2$ in the form $x_n = b\phi^\alpha$, where b and α are two positive numbers to be determined. When we replace this ansatz into Eq. $(46)_2$ and discard negligible terms, we arrive at

$$\frac{b}{\vartheta_c}\phi^\alpha \left[\frac{b}{\vartheta_c}\phi^\alpha - \phi \sin^2 \vartheta_c \right] = 0$$

whence $\alpha = 1$ and $b = \vartheta_c \sin^2 \vartheta_c$ follow. Fig. 8 points out a difference between peristaltic and varicose modes since for these latter the marginal curves emanate from a precise point $\phi(\vartheta_c)$ of the ϕ axis: $\phi(65°) = 2.66$. As for peristaltic modes, as soon as a non-vanishing value for η is fixed, the marginal curve diverges along the ϱ_n axis (*see* the semi-logarithmic plot shown in Fig. 9) confirming the stabilizing rôle of curvature corrections. The same regimes discussed for peristaltic modes exist here, apart from the absence of Rayleigh instability when $\phi > \phi(\vartheta_c)$.

Figure 10 shows the stability diagram when $\vartheta_c = 125°$. As already discussed for peristaltic modes, there are no essential differences with respect to the case in which the contact angle ϑ_c is less than $\pi/2$. Similar remarks hold for the semi-logarithmic counterpart shown in Fig. 11. Finally, Figure 12 shows the critical value of $\eta_c(\vartheta_c)$ at which the marginal curve follows a monotonic profile: it has the same qualitative behaviour as that computed for peristaltic modes.

5 Conclusions

We determined the effects of a curvature correction to line tension on both the equilibrium and the stability of sessile droplets through a general variational analysis. While the effects on the equilibrium could be even absent, those on stability are relevant in any case. As a first consequence, we proved for liquid bridges that the curvature correction makes wildly oscillating perturbations unrewarding, and so the systematic instability against all modes with short wavelength induced by negative line tensions is removed, regardless of the magnitude of the correction. This magnitude, however, plays a crucial rôle in determining whether only Rayleigh instability occurs or not. As a general result,

Rayleigh instability is the only destabilizing mechanism whenever the curvature correction is large enough. The analysis employed here for liquid bridges could serve to explore the stabilizing effects of curvature corrections on droplets with a closed geometry.

6 Appendix: Second variation of $\mathcal{F}^*$

We show in detail how to obtain the expression (19) for the second variation $\delta^2\mathcal{F}^*$ of $\mathcal{F}^*$, obtained by integrating along $\mathcal{C}$ the terms in (14) that are quadratic in ε. We start with

$$\mathcal{I}_1 := \int_{\mathcal{C}} [2\sigma \boldsymbol{c}' \cdot \boldsymbol{n} - \sigma' \boldsymbol{v} \cdot \boldsymbol{t}] \mathrm{d}s$$

which contains contributions related to the field $\boldsymbol{v}$ defined in Eq. (6). The integral $\mathcal{I}_1$ has the same structure as the first variation of $\mathcal{F}^*$ given in (15), with $\boldsymbol{u}$ and $\boldsymbol{a}$ replaced by $\boldsymbol{v}$ and $\boldsymbol{c}$. The crucial difference in this formal change is that, at variance with $\boldsymbol{u}$, the field $\boldsymbol{v}$ has also a non trivial component along the unit normal vector $\boldsymbol{\nu}_*$ of $\mathcal{S}_*$. By retracing the same steps as in Sec. 3, we can check that the component $\boldsymbol{v} \cdot \boldsymbol{t}$ does not contribute and the component along $\boldsymbol{\nu}_{\mathcal{S}_*}$ vanishes by virtue of the equilibrium equation (18). Hence, we are left with the component $\boldsymbol{v} \cdot \boldsymbol{\nu}_*$ which, by use of $(7)_2$, can be recast as

$$\mathcal{I}_1 = -\int_{\mathcal{C}} \frac{1}{2}\boldsymbol{u}\cdot(\nabla_s\boldsymbol{\nu}_*)\boldsymbol{u}[\sigma^2\kappa_n + 2\kappa_n'' - 4\tau_g\kappa_g' - 2\kappa_g\tau_g' - 2\kappa_n\tau_g^2]\mathrm{d}s\,,$$

where perusal of Darboux equations (8) has been made. By recalling that [25]

$$\nabla_s\boldsymbol{\nu}_* = -\kappa_n\boldsymbol{t}\otimes\boldsymbol{t} - \kappa_{n\perp}\boldsymbol{\nu}_{\mathcal{S}}\otimes\boldsymbol{\nu}_{\mathcal{S}} + \tau_g(\boldsymbol{\nu}_{\mathcal{S}}\otimes\boldsymbol{t} + \boldsymbol{t}\otimes\boldsymbol{\nu}_{\mathcal{S}})\,, \tag{47}$$

where $\kappa_{n\perp} := H - \kappa_n$ is expressed in terms of the total curvature H of $\mathcal{S}_*$, we finally arrive at

$$\mathcal{I}_1 = \int_{\mathcal{C}} \frac{1}{2}[\kappa_n u_t^2 - 2\tau_g u_t u_s + (H - \kappa_n)u_s^2]\{\sigma^2\kappa_n + 2\kappa_n'' - 4\tau_g\kappa_g' - 2\kappa_g\tau_g' - 2\kappa_n\tau_g^2\}\mathrm{d}s\,, \tag{48}$$

It is also expedient to expand $\boldsymbol{u}'$ and $\boldsymbol{a}$ along the Darboux trihedron of $\mathcal{C}$, by resorting to Eqs. (8), $(10)_1$ and (17):

$$\boldsymbol{u}' = (u_t' - \kappa_g u_s)\boldsymbol{t} + (u_s' + \kappa_g u_t)\boldsymbol{\nu}_{\mathcal{S}} + (\kappa_n u_t - \tau_g u_s)\boldsymbol{\nu} \tag{49}$$

and

$$\boldsymbol{a} = (u_s' + \kappa_g u_t)\boldsymbol{\nu}_{\mathcal{S}} + (\kappa_n u_t - \tau_g u_s)\boldsymbol{\nu} \tag{50}$$

from which

$$a^2 = u_t^2\sigma^2 + u_s'^2 + \tau_g^2 u_s^2 + 2\kappa_g u_t u_s' - 2\tau_g\kappa_n u_t u_s$$

easily follows. By differentiating $\boldsymbol{a}$ with respect to s we also obtain, by Eq. (8),

$$\boldsymbol{a}' = [\kappa_n\tau_g u_s - \kappa_g u_s' - \sigma^2 u_t]\boldsymbol{t} + [(u_s' + \kappa_g u_t)' + \tau_g(\kappa_n u_t - \tau_g u_s)]\boldsymbol{\nu}_{\mathcal{S}} +$$
$$+[(\kappa_n u_t - \tau_g u_s)' - \tau_g(u_s' + \kappa_g u_t)]\boldsymbol{\nu} \tag{51}$$

whence, after straightforward computations also involving differentiation of the identity (17), we arrive at

$$\mathcal{I}_2 := \int_{\mathcal{C}} \boldsymbol{a}' \cdot \boldsymbol{a}' \mathrm{d}s = \int_{\mathcal{C}} [\sigma^4 + (\kappa_g')^2 + (\kappa_n')^2 + \sigma^2\tau_g^2 + 2\tau_g(\kappa_n\kappa_g' - \kappa_g\kappa_n')]u_t^2 +$$

$$+ \int_{\mathcal{C}} (\sigma^2)' u_t u_t' + \int_{\mathcal{C}} \sigma^2 (u_t')^2 \mathrm{d}s + \int_{\mathcal{C}} 2[\kappa_g\sigma^2 - 2\tau_g(\kappa_n' - \tau_g\kappa_g)]u_t u_s' -$$

$$- \int_{\mathcal{C}} 2[\kappa_n\tau_g\sigma^2 + \tau_g^2(\kappa_g' + \kappa_n\tau_g) + \tau_g'(\kappa_n' - \tau_g\kappa_g)]u_t u_s - \int_{\mathcal{C}} 2[\tau_g(\kappa_n\kappa_g + 2\tau_g')]u_s u_s' +$$

$$+ \int_{\mathcal{C}} (\kappa_g^2 + 4\tau_g^2)(u_s')^2 + \int_{\mathcal{C}} [(\kappa_n\tau_g)^2 + \tau_g^4 + (\tau_g')^2]u_s^2 + \int_{\mathcal{C}} (u_s'')^2 + \int_{\mathcal{C}} 2\kappa_g u_t' u_s'' -$$

$$- \int_{\mathcal{C}} 2[\kappa_g\tau_g^2 + \tau_g'\kappa_n]u_s u_t' + \int_{\mathcal{C}} 2[\kappa_g' + \kappa_n\tau_g]u_t u_s'' - \int_{\mathcal{C}} 2\tau_g^2 u_s u_s'' - \int_{\mathcal{C}} 4\tau_g\kappa_n u_s' u_t'.$$

$$(52)$$

To proceed, we consider the terms

$$\mathcal{I}_3 := \int_{\mathcal{C}} \sigma^2[(\boldsymbol{u}' \cdot \boldsymbol{t})^2 - \frac{3}{2}a^2]\mathrm{d}s,$$

that, by use of Eqs. (49-50) can be recast as

$$\mathcal{I}_3 = \int_{\mathcal{C}} \sigma^2(u_t')^2 + \int_{\mathcal{C}} \sigma^2(\kappa_g^2 - \frac{3}{2}\tau_g^2)u_s^2 - \int_{\mathcal{C}} 2\kappa_g\sigma^2 u_s u_t' - \int_{\mathcal{C}} \frac{3}{2}\sigma^4 u_t^2 - \int_{\mathcal{C}} \frac{3}{2}\sigma^2(u_s')^2 -$$

$$- \int_{\mathcal{C}} 3\sigma^2\kappa_g u_t u_s' + \int_{\mathcal{C}} 3\kappa_n\tau_g\sigma^2 u_t u_s.$$

$$(53)$$

Finally, by integration by parts we change

$$\mathcal{I}_4 := -2 \int_{\mathcal{C}} [(\boldsymbol{u}' \cdot \boldsymbol{t})'\sigma\boldsymbol{n} \cdot \boldsymbol{a} + 2(\boldsymbol{u}' \cdot \boldsymbol{t})\boldsymbol{a}' \cdot \sigma\boldsymbol{n}]\mathrm{d}s$$

into

$$\mathcal{I}_4 = 2 \int_{\mathcal{C}} \boldsymbol{a} \cdot \sigma\boldsymbol{n}(\boldsymbol{u}' \cdot \boldsymbol{t})'\mathrm{d}s + 4 \int_{\mathcal{C}} \boldsymbol{a} \cdot (\sigma\boldsymbol{n})'(\boldsymbol{u}' \cdot \boldsymbol{t})\mathrm{d}s$$

which, also by use of Eqs. $(8)_1$, (17), and (49), yields

$$\mathcal{I}_4 = \int_{\mathcal{C}} 2\sigma^2 u_t u_t'' + \int_{\mathcal{C}} 2\kappa_g u_s' u_t'' - \int_{\mathcal{C}} 2\kappa_n\tau_g u_s u_t'' + \int_{\mathcal{C}} 4[(\kappa_g' + \kappa_n\tau_g)]u_t' u_s' -$$

$$-2 \int_{\mathcal{C}} \kappa_g^2(u_s')^2 - \int_{\mathcal{C}} 2[\kappa_g[\kappa_n\tau_g + 3\kappa_g']]u_s u_s' + \int_{\mathcal{C}} 2[\kappa_g'\kappa_n\tau_g - 2\kappa_g(\kappa_g\tau_g^2 - \tau_g\kappa_n')]u_s^2 -$$

$$- \int_{\mathcal{C}} 2(\sigma^2\kappa_g)' u_s u_t + \int_{\mathcal{C}} 2(\sigma^2)' u_t u_t' + \int_{\mathcal{C}} 4(\kappa_g\tau_g - \kappa_n')\tau_g u_t' u_s - 2 \int_{\mathcal{C}} \kappa_g\sigma^2 u_t u_s'.$$

$$(54)$$

As already mentioned for $\delta\mathcal{F}^*$, the component u_t cannot appear in the final expression of $\delta^2\mathcal{F}^*$. To prove this, we collect terms in $\delta^2\mathcal{F}^*$ with the same dependence on u_t and its derivatives with respect to s, and integrate repeatedly by parts.

- Terms containing $u_t'^2$ and $u_t u_t''$ in $\mathcal{I}_3$ and $\mathcal{I}_4$ are

$$2 \int_{\mathcal{C}} \sigma^2(u_t'^2 + u_t u_t'')\mathrm{d}s = -2 \int_{\mathcal{C}} (\sigma^2)' u_t u_t' \mathrm{d}s$$

$$(55)$$

21

that are combined with the term $3\int_{\mathcal{C}}\sigma^2 u_t u_t' \mathrm{d}s$ found in $\mathcal{I}_2$ and $\mathcal{I}_4$ to obtain, by Eq. (17),

$$\int_{\mathcal{C}}(\sigma^2)' u_t u_t' \mathrm{d}s = -\frac{1}{2}\int_{\mathcal{C}}(\sigma^2)'' u_t^2 \mathrm{d}s = -\int_{\mathcal{C}}(\kappa_g'^2 + \kappa_n'^2 + \kappa_g \kappa_g'' + \kappa_n \kappa_n'') u_t^2 \mathrm{d}s\,. \tag{56}$$

• Further terms containing u_t^2 in $\mathcal{I}_1$-$\mathcal{I}_3$ are collected together to yield, also by use of Eq. (17),

$$\int_{\mathcal{C}}[-\frac{\sigma^4}{2} + (\kappa_g')^2 + (\kappa_n')^2 + \tau_g^2 \kappa_g^2 - 2\tau_g \kappa_g \kappa_n' + \frac{\sigma^2}{2}\kappa_n^2 + \kappa_n \kappa_n'' - \kappa_g \kappa_n \tau_g'] u_t^2 \mathrm{d}s$$

that, when added to (56), gives

$$\int_{\mathcal{C}}[-\frac{\sigma^4}{2} + \frac{\kappa_g}{2}(2\kappa_g \tau_g^2 - 4\tau_g \kappa_n' - 2\kappa_g'' - 2\kappa_n \tau_g') + \frac{\sigma^2}{2}\kappa_n^2] u_t^2 \mathrm{d}s\,. \tag{57}$$

Now, terms in u_t should simplify separately for each integral in $\mathcal{F}$. Hence, we can use the reduced equilibrium equation

$$\kappa_g \sigma^2 + 2(\tau_g' \kappa_n + 2\tau_g \kappa_n' + \kappa_g'' - \kappa_g \tau_g^2) = 0\,, \tag{58}$$

obtained by setting $\delta\mathcal{F}^* = 0$ together with Eq. (17) to show that the integral (57) vanishes identically on any equilibrium configuration.

We now prove that mixed terms containing products of u_t and u_s or of their derivatives do not enter in $\delta^2\mathcal{F}^*$.

• The terms in $\mathcal{I}_2$ containing the product $u_t u_s''$ can be transformed via integration by parts as

$$2\int_{\mathcal{C}}(\kappa_g' + \kappa_n \tau_g) u_t u_s'' \mathrm{d}s = -2\int_{\mathcal{C}}(\kappa_g' + \kappa_n \tau_g) u_t' u_s' \mathrm{d}s - 2\int_{\mathcal{C}} u_t u_s'(\kappa_g'' + \kappa_n' \tau_g + \kappa_n \tau_g') \mathrm{d}s$$

to which we add the term in $\mathcal{I}_4$

$$2\int_{\mathcal{C}}\kappa_g u_t'' u_s' \mathrm{d}s = -2\int_{\mathcal{C}}(\kappa_g u_s'' u_t' + \kappa_g' u_s' u_t') \mathrm{d}s\,,$$

containing $u_t'' u_s'$ and then add the term in $\mathcal{I}_2$ that contains $u_s'' u_t'$: as a result, we are left with

$$-2\int_{\mathcal{C}}(2\kappa_g' + \kappa_n \tau_g) u_t' u_s' \mathrm{d}s - 2\int_{\mathcal{C}} u_t u_s'(\kappa_g'' + \kappa_n' \tau_g + \kappa_n \tau_g') \mathrm{d}s\,. \tag{59}$$

Since the remaining terms in $\mathcal{I}_2$ and $\mathcal{I}_4$ containing $u_t' u_s'$ reduce to

$$4\int_{\mathcal{C}}\kappa_g' u_t' u_s' \mathrm{d}s$$

we finally arrive at

$$-2\int_{\mathcal{C}}\{[\kappa_g'' + (\tau_g \kappa_n)'] u_t u_s' + \kappa_n \tau_g u_t' u_s'\} \mathrm{d}s\,. \tag{60}$$

- The term

$$-2 \int_{\mathcal{C}} \kappa_n \tau_g u_s u_t'' \mathrm{d}s = 2 \int_{\mathcal{C}} [\kappa_n \tau_g u_t' u_s' + (\kappa_n \tau_g)' u_s u_t'] \mathrm{d}s \,,$$

of $\mathcal{I}_4$ can be added to the integral (60), to arrive at

$$2 \int_{\mathcal{C}} \{u_s u_t' (\kappa_n \tau_g)' - [\kappa_g'' + (\kappa_n \tau_g)'] u_t u_s'\} \mathrm{d}s \,, \tag{61}$$

or, after integration by parts, at

$$-2 \int_{\mathcal{C}} \{u_s u_t (\kappa_n \tau_g)'' + u_t u_s' [\kappa_g'' + 2(\kappa_n \tau_g)']\} \mathrm{d}s \,. \tag{62}$$

- We then consider the following terms in $\mathcal{I}_2$-$\mathcal{I}_4$ that contain $u_t' u_s$

$$2 \int_{\mathcal{C}} u_t' u_s [\kappa_g \tau_g^2 - \tau_g' \kappa_n - \kappa_g \sigma^2 - 2\tau_g \kappa_n'] \mathrm{d}s$$

and integrate them by parts obtaining

$$2 \int_{\mathcal{C}} \{u_s' u_t [-\kappa_g \tau_g^2 + \tau_g' \kappa_n + \kappa_g \sigma^2 + 2\tau_g \kappa_n'] + u_t u_s [\tau_g' \kappa_n + \kappa_g \sigma^2 + 2\tau_g \kappa_n' - \kappa_g \tau_g^2]'\} \mathrm{d}s \,. \tag{63}$$

- Further integrals containing $u_s' u_t$ in $\mathcal{I}_2$-$\mathcal{I}_4$ are collected to give

$$-\int_{\mathcal{C}} [3\kappa_g \sigma^2 + 4\tau_g (\kappa_n' - \tau_g \kappa_g)] u_s' u_t \mathrm{d}s \tag{64}$$

that, after algebraic manipulations and use of (58), when added to (62) and (63) yield

$$2 \int_{\mathcal{C}} u_s u_t \{[\tau_g' \kappa_n + \kappa_g \sigma^2 + 2\tau_g \kappa_n' - \kappa_g \tau_g^2]' - (\kappa_n \tau_g)''\} \mathrm{d}s$$

that simplifies to zero when it is added to the remaining terms in $\mathcal{I}_1 - \mathcal{I}_4$ containing $u_s u_t$, namely,

$$2 \int_{\mathcal{C}} u_s u_t [\tau_g^2 \kappa_g' + 2\tau_g \tau_g' \kappa_g - \tau_g' \kappa_n' - (\kappa_g \sigma^2)' - \kappa_n'' \tau_g] \mathrm{d}s \,,$$

as can be easily checked.

Hence, we proved that only terms containing u_s'', u_s' and u_s appear in the second variation of $\mathcal{F}^*$. Precisely, we can recast $\delta^2 \mathcal{F}^*$ into a diagonal form in which only $(u_s'')^2$, $(u_s')^2$, and $(u_s)^2$ appear.

- In $\mathcal{I}_2$ we consider the terms

$$\int_{\mathcal{C}} [(u_s'')^2 - 2\tau_g^2 u_s u_s''] \mathrm{d}s = \int_{\mathcal{C}} \{(u_s'')^2 + 2\tau_g^2 (u_s')^2 + 4\tau_g \tau_g' u_s u_s'\} \mathrm{d}s$$

that, when added to the remaining terms in $\mathcal{I}_2$-$\mathcal{I}_4$ containing $(u_s')^2$, yield

$$\int_{\mathcal{C}} \{(u_s'')^2 + (6\tau_g^2 - \kappa_g^2 - \frac{3}{2}\sigma^2)(u_s')^2 + 4\tau_g \tau_g' u_s u_s'\} \mathrm{d}s \,. \tag{65}$$

23

• We now add to (65) the terms in $\mathcal{I}_2$ and $\mathcal{I}_4$ with $u_s u_s'$ arriving at

$$\int_{\mathcal{C}}\{(u_s'')^2 + (6\tau_g^2 - \kappa_g^2 - \frac{3}{2}\sigma^2)(u_s')^2 - 2[2\tau_g\kappa_g\kappa_n + 3\kappa_g\kappa_g']u_s u_s'\}\mathrm{d}s. \qquad (66)$$

Finally, if we add the remaining contributions in $\mathcal{I}_1$-$\mathcal{I}_4$ that contain u_s^2 and then integrate by parts the last term in (66), we obtain the expression (19) for $\delta^2\mathcal{F}^*$.

Acknowledgements

References

[1] J.W. GIBBS, On the equilibrium of heterogeneous substances, in The Collected Papers of J. Willard Gibbs Vol. I, Yale University Press, London, 1957, pp.55-353.

[2] R. TOLMAN, The effect of droplet size on surface tension, J. Chem. Phys., 17(1949), pp. 333-337.

[3] M.J.P. NIJMEIJER, C. BRUIN, A.B. VAN WOERKOM, A.F. BAKKER, J.M.J. VAN LEEUWEN, Molecular dynamics of the surface tension of a drop, J. Chem. Phys., 96(1992), pp. 565-576.

[4] E.M. BLOCKHUIS, D. BEDEAUX, Pressure tensor of a spherical interface, J. Chem. Phys., 97(1992), pp. 3576-3586.

[5] E.M. BLOCKHUIS, D. BEDEAUX, Derivation of microscopic expressions for the rigidity constants of a simple liquid vapor interface, Physica A, 184(1992), 42–70 .

[6] V.G. BAIDAKOV, G. Sh. BOLTACHEV, and G.G. CHERNYKH, Curvature corrections to surface tension, Phys. Rev. E, 70(2004), 011603.

[7] P.S. SWAIN and R. LIPOWSKY, Contact angles on heterogeneous substrates: a new look at Cassie's and Wenzel's laws, Langmuir, 14(1998), pp. 6772–6780.

[8] R. LIPOWSKY, P. LENZ, and P.S. SWAIN, Wetting and dewetting of structured and imprinted surfaces, Colloid Surface A, 161(2000), pp. 3-22.

[9] D.J. STEIGMANN and D. LI, Energy-minimizing states of capillary systems with bulk, surface, and line phases, IMA J. Appl. Math., 55(1995), pp. 1-17.

[10] Y. SOLOMENTSEV, L.R. WHITE, Microscopic drop profiles and the origins of line tension, J. Colloid Interf. Sci., 218(1999), pp. 122–136.

[11] J.S. ROWLINSON, B. WIDOM, Molecular Theory of Capillarity, Dover, New York, 2002.

[12] R. ROSSO and E.G. VIRGA, A general stability criterion for wetting, Phys. Rev. E, 68(2003), 012601.

[13] R. ROSSO and E.G. VIRGA, Local stability for a general wetting functional, J. Phys. A-Math. Gen., 37(2004), pp. 3989-4015. Corrigendum, *ibid.*, 37(2004), p. 8751.

[14] M. BRINKMANN, J. KIERFELD, and R. LIPOWSKY, A general stability criterion for droplets on structured substrates, J. Phys. A-Math. Gen., 37(2004), pp. 11547-11573.

[15] R. ROSSO and E.G. VIRGA, Sign of line tension in liquid bridge stability, Phys. Rev. E, 70(2004), 031603.

[16] M. BRINKMANN, J. KIERFELD, and R. LIPOWSKY, Stability of liquid channels or filaments in the presence of line tension, J. Phys.-Condens. Mat., 17(2005), pp. 2349-2364.

[17] L. GUZZARDI, R. ROSSO, E.G. VIRGA, Residual stability of sessile droplets with negative line tension, Phys. Rev. E, 73(2006), 021602.

[18] L. GUZZARDI, R. ROSSO, Sessile droplets on a curved substrate: effects of line tension, J. Phys. A Math. and Theor., 40(2007), pp. 19–46.

[19] J.Y. WANG, S. BETELU, M. LAW, Line tension approaching a first-order wetting transition: experimental results from contact angle measurements, Phys. Rev. E, 63(2001), 031601.

[20] L. BORUVKA, and A.W. NEUMANN, Generalization of the classical theory of capillarity, J. Chem. Phys., 66(1977), pp. 5464–5476.

[21] A.I. RUSANOV, A.K. SHCHEKIN, D.V. TATYANENKO, The line tension and the generalized Young equation: the choice of dividing surface, Coll. Surfaces A: Physicochem. Eng. Aspects, 250(2004), pp. 263–268.

[22] P.JAKUBCZYK, M. NAPIÓRKOWSKI, Influence of inhomogeneous substrate curvature on line tension, Phys. Rev. E, 72(2005), 011603.

[23] T. BIEKER, S. DIETRICH, Wetting of curved substrates, Physica A, 252(1998), pp. 85–137.

[24] M.P. DO CARMO, Differential Geometry of Curves and Surfaces, Prentice-Hall, Englewood-Cliffs, 1976.

[25] R. ROSSO, Curvature effects in vesicle-particle interactions, Proc. R. Soc. London A, 459(2003), pp. 829-852.

[26] C.M. BENDER, S.A. Orszag Advanced Mathematical Methods for Scientists and Engineers. Asymptotic Methods and Perturbation Theory, Springer, Heidelberg, 1999.
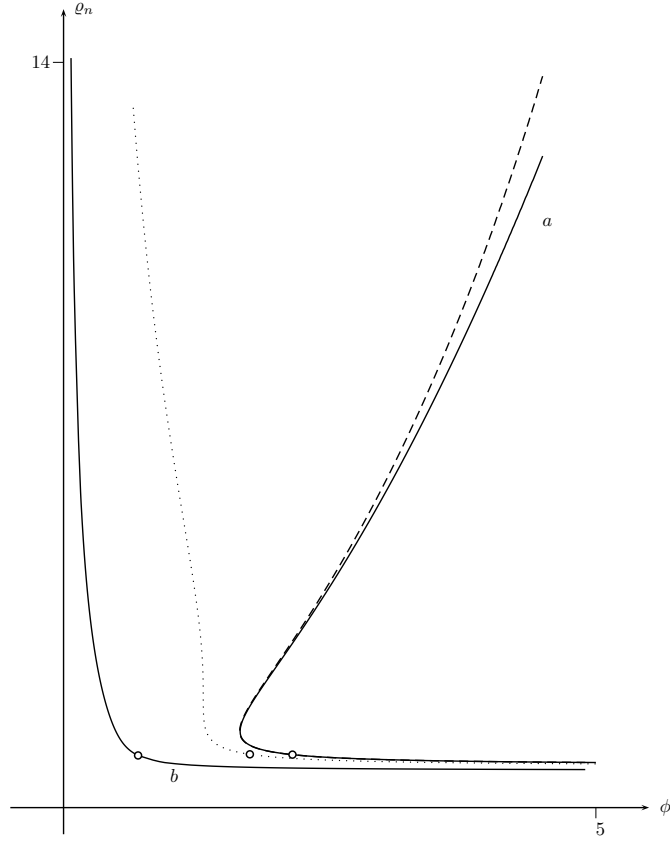
Figure 6: Stability diagram against peristaltic modes when $\vartheta_c = 125°$, for several values of η: $\eta = 0$ (solid line a), 10^{-3} (dashed line), 10^{-1} (dotted line), 1 (solid line b). Here, both circular and hyperbolic modes are effective. The portion of a given marginal curve that lies above the circle consists of hyperbolic modes, while the portion below the circle consists of circular modes. Linear modes never affect the stability diagram. Apart from the presence of two families of modes, there is no qualitative difference with respect to the case $\vartheta_c < \pi/2$.
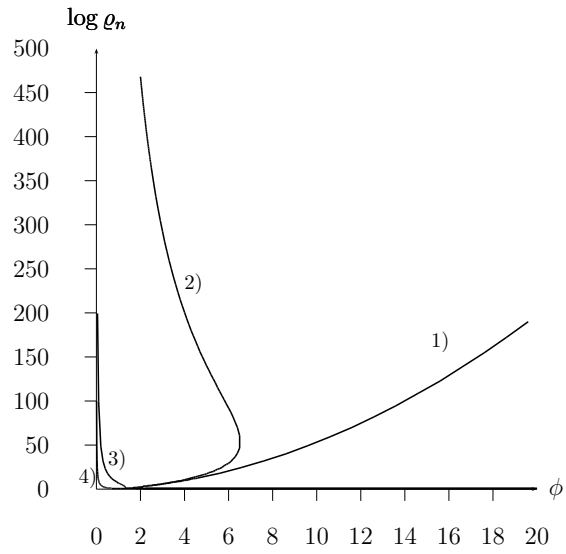
Figure 7: Semi-logarithmic plot of the stability diagram for peristaltic modes shown in Fig. 6. The curves 1)-4) correspond, respectively, to the values $\eta = 0$, 10^{-3}, 10^{-1}, and 1.

27
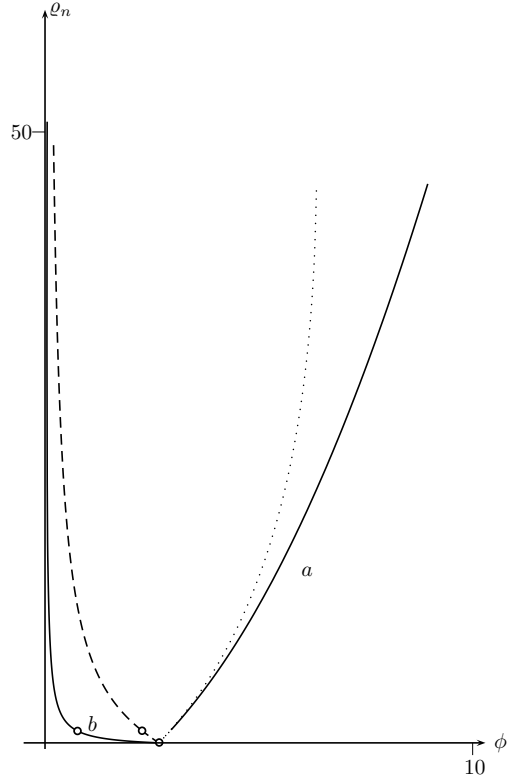
Figure 8: Stability diagrams for varicose—both circular and hyperbolic—modes. Here, $\vartheta_c = 65°$ and $\eta = 0$ (solid line a), 10^{-3} (dotted line), 10^{-1} (dashed line), 1 (solid line b). The portion of a given marginal curve that lies above the circle consists of hyperbolic modes, while the portion below the circle consists of circular modes. The marginal curves coalesce along the ϕ axis, since $\varrho_n = 0$ always solves Eq. $(46)_1$. This solution does not cause instability since only positive values of ϱ_n are meaningful. For any given value of η the region bounded by the marginal curve and the ϱ_n-axis is unstable against varicose modes.
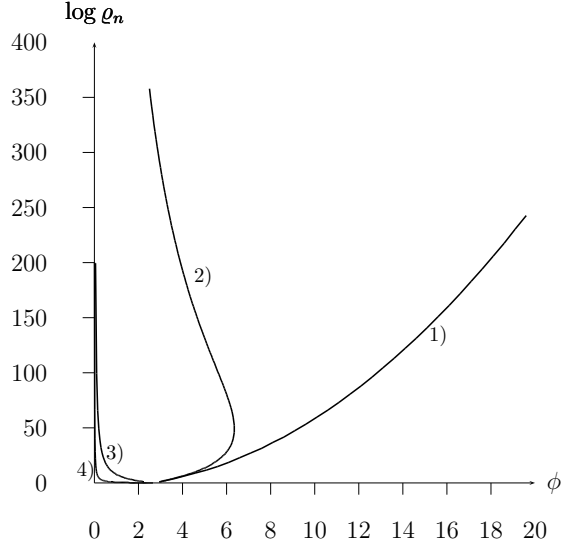
Figure 9: Semi-logarithmic plot of the stability diagrams for varicose modes shown in Fig. 8. From 1) to 4), the marginal curves correspond to $\eta = 0$, 10^{-3}, 10^{-1}, and 1.
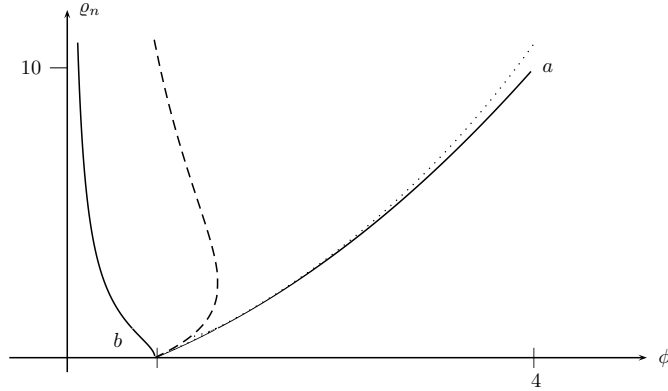
Figure 10: Stability diagram against varicose modes when $\vartheta_c = 125°$, for several values of η: $\eta = 0$ (solid line a), 10^{-3} (dotted line), 10^{-1} (dashed line), 1 (solid line b). Both circular and hyperbolic modes are effective, but the transition between them is too close to the ϕ axis to be shown here. Linear modes never affect the stability diagram. Also in this case, there is a correspondence with the the case $\vartheta_c < \pi/2$.

29
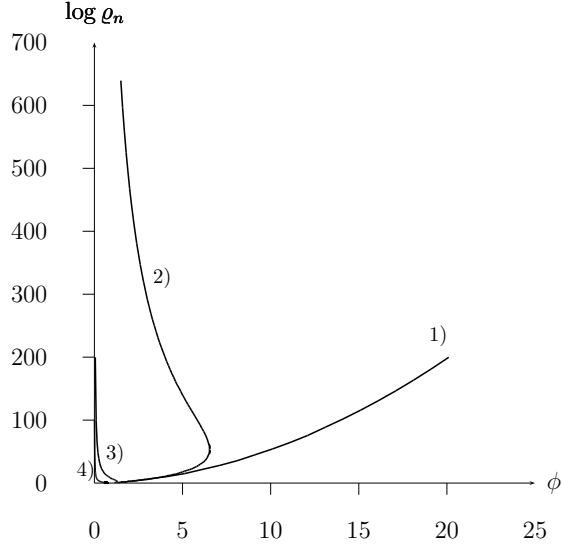
Figure 11: Semi-logarithmic plot of the stability diagrams for varicose modes shown in Fig. 10. From right to left, the marginal curves correspond to $\eta = 0$, 10^{-3}, 10^{-1}, and 1.
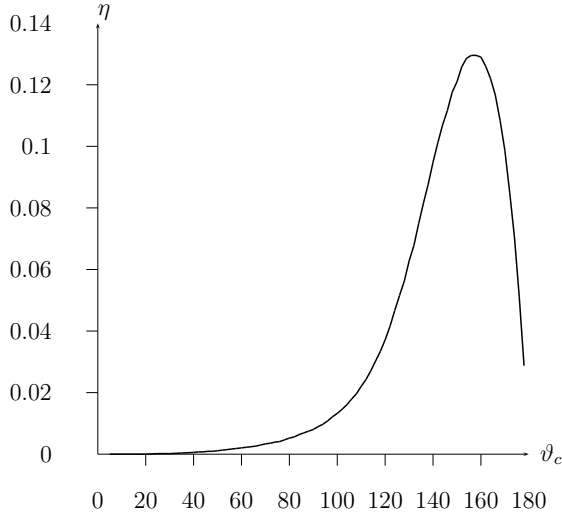
Figure 12: The critical value η_c of η is plotted against the contact angle ϑ_c for varicose modes. When η exceeds η_c, the marginal curve is a monotonic function of ϕ.

30

MOX Technical Reports, last issues

Dipartimento di Matematica "F. Brioschi",
Politecnico di Milano, Via Bonardi 9 - 20133 Milano (Italy)

1/2008   R. Rosso, M. Verani:
Stabilizing rôle of a curvature correction to line tension

26/2007   M. Colecchia, N. Nicolai, P. Secchi, G. Bandieramonte,
A.M. Paganoni, L.M. Sangalli, L. Piva, R. Salvioni:
Penile Superficial Squamous cell Carcinoma (SCC) Submitted to CO_2
Laser Excision only: Oncologic Outcome of T1 Disease in 25 Years-
Long Experience

25/2007   S. Micheletti, S. Perotto:
Space-Time Adaption for Advection-Diffusion-Reaction Problems on
Anisotropic Meshes

24/2007   L.M. Sangalli, P. Secchi, S. Vantini, A. Veneziani:
A Case Study in Functional Data Analisys: Geometrical Features of
the Internal Carotid Artery

23/2007   L.M. Sangalli, P. Secchi, S. Vantini, A. Veneziani:
Efficient estimation of 3-dimensional centerlines of inner carotid ar-
teries and their curvature functions by free knot regression splines

22/2007   G.O. Roberts, L.M. Sangalli:
Latent diffusion models for event history analysis

21/2007   P. Massimi, A. Quarteroni, F. Saleri, G. Scrofani:
Modeling of Salt Tectonics

20/2007   E. Burman, A. Quarteroni, B. Stamm:
Stabilization Strategies for High Order Methods for Transport Domi-
nated Problems

19/2007   E. Burman, A. Quarteroni, B. Stamm:
Interior Penalty Continuous and Discontinuous Finite Element
Approximations of Hyperbolic Equations

18/2007   S. Micheletti, S. Perotto:
Output functional control for nonlinear equations driven by anisotropic
mesh adaption. The Navier-Stokes equations